J Radioanal Nucl Chem (2016) 310:125–137
DOI 10.1007/s10967-016-4779-4

Dihydroxy bezladely derivatives functionalized mesoporous silica SBA-15 for the sorption of U(VI)

Lu Zhu[1] · Yalou Sun[1] · Lijuan Song[1] · Xiangchen Shi[1] · Su-Wen Chen[1] · Wangsuo Wu[1]

Received: 17 November 2015 / Published online: 9 March 2016

Abstract Three different modified SBA-15 have been synthesized by a post-grafting method using 3,4-dihydroxy benzaldehyde (OHBA), 2,4-dihydroxy benzaldehyde (MHBA), 2,4-dihydroxy acetophenone (RATP). These materials were characterized by NMR, TEM, FT-IR and elemental analysis. Batch experiments have been conducted to study the effects of pH, temperature, adsorbent dosage, ionic strength, shaking time, initial concentration of metal ion, and coexisting ions on uranium(VI) sorption behaviors of pure and functional SBA-15. In addition, the adsorption of U(VI) could be well-described by the Langmuir, Freundlich isotherms and pseudo-second kinetic models. The results suggest the sorption capacity and selectivity of SBA-15 were improved after functionalization.

Keywords Mesoporous silica · Uranium(VI) · Adsorption · Dihydroxy benzaldehyde · Post-grafting

Introduction

In recent years, a shift towards renewable energy supplies is urgently needed in order to sustain global economic growth and mitigate the climate change caused by burning fossil fuels [1] so as to decrease the level of the atmospheric carbon dioxide. Nuclear energy is an only mature, clean and large-scale power to satisfy the growing energy demand in the future. With rapid development and large utilization of nuclear power, uranium is one of the main radionuclides in nuclear industry [2] which starts as a source and ends up as a radioactive waste component [3]. Owing to its chemical and radio toxicity, uranium is one of major concern with regard to environmental clean up [4, 5]. Uranium can cause potentially serious health hazards to humans if it was released into soil and water bodies [6, 7].

The efficient methods for removal of uranium from wastes are imperative. Until now, a variety of methods have been developed for uptake of uranium, such as ion exchange, chemical precipitation, co-precipitation, solvent extraction, chromatographic extraction, hyperfiltration and adsorption [8–12]. Among them, sorption is a widely used method as regard to its easy-operation, rapidity, and high-efficiency [13, 14].

Because mesoporous silicas with well-ordered pore channels are currently the focus of a great deal of research interest [15–18]. Ordered mesoporous silicas have high porosities, large surface areas, excellent mechanical property, and adjustable pore size. They are usually used as adsorbents for the separation of organics, heavy metal ions, dyes, radionuclides, light hydrocarbons, and gases [19, 20]. Among them, SBA-15 mesoporous silica material possesses thicker pore walls, larger pore volume, high surface area and better hydrothermal stabilities, so it is usually chosen as a potential sorption material for some heavy metal ion sorption. At the same time, low chemical activity of the SBA-15 should be taken into account, which could decrease the sorption ability of SBA-15. In recent years, in order to improve the sorption ability and selectivity, many people have functionalized SBA-15 with organic groups. Wang YL et al. reported that mesoporous silica SBA-15 functionalized with iminodiacetic acid derivatives have a good sorption ability and selectivity for UO_2^{2+} from aqueous solution [21]. Mesoporous silica modified with 2-mercaptopyrimidine showed excellent adsorption capability for Cd(II) [22].

✉ Su-Wen Chen
chensuwen@lzu.edu.cn

[1] School of Nuclear Science and Technology, Lanzhou University, Lanzhou 730000, People's Republic of China

Mureseanu et al. reported that Mesoporous silica functionalized with 1-furoyl thiourea urea for Hg(II) adsorption from aqueous media [23]. Phosphonate derivatives functionalized SBA-15 material showed not only a good sorption ability and a desirable selectivity for U(VI) over a range of competing metal ions but also an excellent reusability [24], and 1,2-formylsalicylic acid have a high affinity for lanthanides (La, Ce, Pr, Nd, Eu, Gd and Lu) from aqueous solution [25].

Dihydroxy bezladely derivatives are known to form stable metal complexes with different metal ions in the solid state under proper conditions. Anupama et al. reported that the silica gel functionalized with bezladely derivatives resacetophenone: synthesis of a new chelating matrix and its application as metal ion collector [26]. As reported from previous work [27], silica gel modified with formylsalicylic acid has been used for extraction of iron(III) from aqueous solution. The results showed that high adsorption values are recorded at neutral pH, which may be due to the strong coordination ability of hydroxy benzaldehyde derivatives to metal ions. However, the relevant reports about the sorption of uranium on modified silica by dihydroxy bezladely derivatives were quite scarce.

Driven by the above realization, we modified SBA-15 to remove uranium by using three dihydroxy bezladely derivatives which are 3,4-dihydroxy benzaldehyde, 2,4-dihydroxy benzaldehyde and 2,4-dihydroxyacetophenone as ligands. The products exhibit high adsorption affinity for U(VI) ions, resulting from complexation of the U(VI) ions by surface dihydroxy bezladely derivatives groups. Furthermore, the effects of different operational parameters on U(VI) adsorption, such as solution adsorbent dosage, pH value, shaking time, and the temperature have been studied. In addition, the adsorption kinetics and thermodynamics have also been investigated. We also compared the selective sorption ability of pure and functional SBA-15 on U(VI) sorption behavior. Additionally, the reports focused on developing SBA-15 modified with dihydroxy bezladely derivatives for U(VI) sorption are quite rare to date, so we anticipate that this work could provide a good example for the removal of U(VI).

Experimental

Reagents and materials

All chemicals used in the experiments are purchased as analytical purity or highest purity available. All solutions are prepared with deionized water by means of a Millipore Milli-Q-system. SBA-15 mesoporous molecular sieve were purchased from Unicarbonshanghai Co. Ltd. Organic solvents (toluene, diethyl ether and ethanol) were distilled and dried before use according to conventional literature methods [22]. 3-aminopropyltriethoxysilane (APTES) and arsenazo III were obtained from Kermel and used as received.

Sorbent synthesis

The dihydroxy bezladely derivatives modified SBA-15 were synthesized by post-grafting methods and the procedures are as follows (Fig. 1).

Preparation for SBA-15-NH_2

SBA-15-NH_2 was synthesized according to the literature methods [28]. 7 g activated SBA-15 which was treated 12 h at 100 °C under vacuum was dispersed in 100 mL anhydrous toluene. After that, 10 mL of APTES was added to the admixture right away at room temperature under N_2 atmosphere, and the resulting mixture was brought to a boiling temperature in a reflux system glass for 9 h with magnetic sticking. After cooling down, the mixture was filtered, and the solid product was washed several times with toluene and ethanol. At last, the solid was dried at 80 °C under vacuum overnight. The product was named SBA-15-NH_2.

Preparation for SBA-15-RATP

SBA-15-RATP was prepared according to a previously described method [30]: 5 g SBA-15-NH_2 was treated with 7.5 g RATP dissolved in 100 mL of dry toluene and the mixture was refluxed with constant stirring for 12 h under nitrogen atomosphere. Rest of the procedure was same as described for SBA-15-NH_2. The synthesis of SBA-15-MHBA and SBA-15-OHBA are conducted in the same way as SBA-15-RATP (see Fig. 1).

Characterization

SAB-15 and functional SBA-15 were characterized by X-ray powder diffraction (XRD), Fourier Transform Infrared Spectrometer FT-IR, nitrogen adsorption and desorption experiments, transmission electron microscopy (TEM), and solid-state magic-angle spinning (MAS) nuclear magnetic resonance (NMR) spectra.

XRD pattern is obtained from a D/Max-2400 X-ray diffractometer equipped with a monochromator, using Cu Kα radiation at a wavelength of 0.154 nm, for 2 h from 1° to 60° with a scan speed of 5° per min. The XRD device is operated at 40 kV and 100 mA. Infrared spectra were collected using a Nexus-670 FT-IR spectrometer in the range of 4000–400 cm^{-1} with a resolution of 4 cm^{-1} by

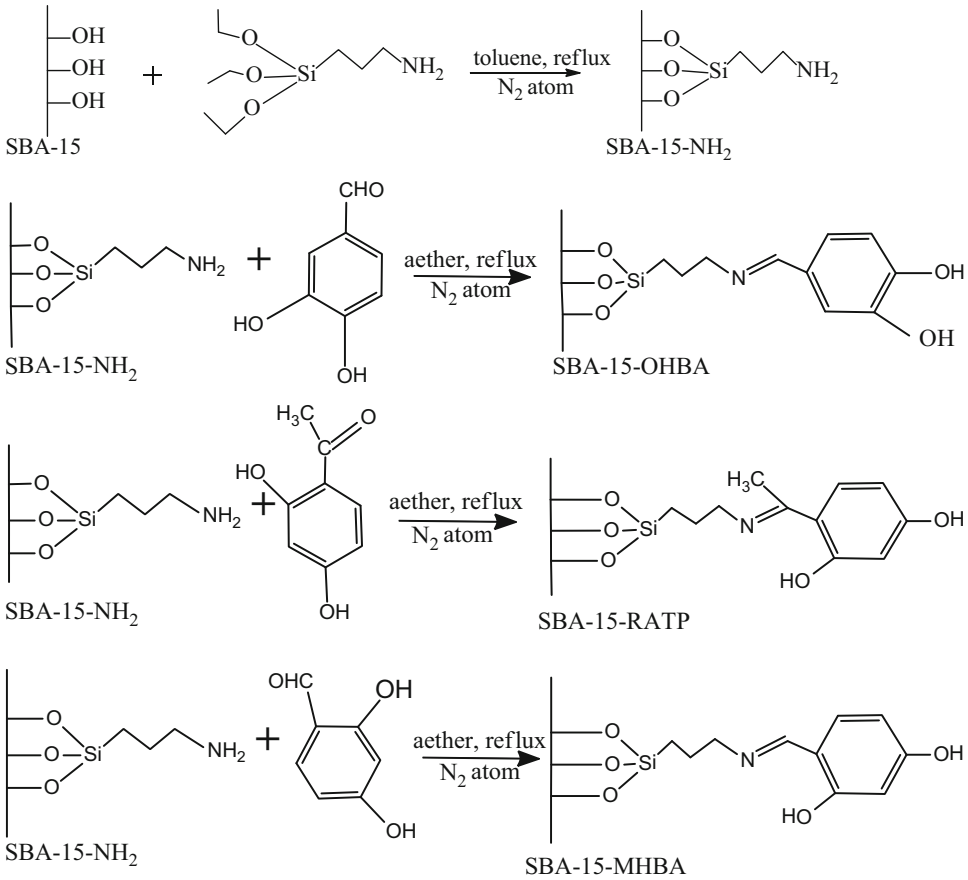

Fig. 1 Schematic illustration of the synthesis process of SBA-15-OHBA, SBA-15-RATP and SBA-15-MHBA

using spectral quality KBr powder. N_2 adsorption–desorption isotherm were conducted using a Micromeritics ASAP 2020 instrument at 77 K. The samples are pretreated at 373 K for 24 h. The pore size was obtained from the maximum of the pore size distribution curve calculated by the Barrett–Joyner–Halenda (BJH) method using the sorption branch of the isotherm. Transmission electron microscopy (TEM) measurements were carried out on a FEI Tecnai F30. Solid-state magic-angle spinning (MAS), nuclear magnetic resonance (NMR) spectra were obtained with a Bruker AV400WB NMR spectrometer with the spinning rate of 10.0 kHz and under magic-angle-spinning (MAS). C, H, and N contents of all samples were measured by combustion oxidation method using a Vario cube elemental analysis apparatus.

Uranium sorption experiment

Batch adsorption experiments were performed to obtain the sorption capacity of U(VI) from aqueous solution of unmodified and modified SBA-15. A representative experiment were carried out by contact of appropriate volume of suspension functionalized SBA-15 sorbent with 0.6 mL $UO_2(NO_3)_2 \cdot 6H_2O$ stock solutions, 0.16 mL $NaNO_3$ solutions (5 mol L^{-1}) and some water (the total volume is 8.00 mL) in polyethylene centrifuge tubes. Then adjusting the pH values of the suspension using negligible volumes of NaOH and HNO_3 solution and the samples were agitated at 25 ± 1 °C for 72 h. After that, the solid and liquid phases are separated by centrifugation with a speed of 10,000 rpm for 30 min (H2050R-1, Xiang Yi Centrifuge Instrument Co. Ltd). Residual U(VI) concentration of the supernatant were analyzed by arsenazo(III) method as a complexing agent at a wavelength of 652 nm [28, 29]. In each set, uranium solution without sorbent was used as a control. Percentage removal and uptake (q) were defined by using the following expressions:

$$q(\%) = \frac{c_0 - c_e}{c_0} \times 100\,\% \quad (1)$$

$$q_e = \frac{c_0 - c_e}{m_s} \times V_s \quad (2)$$

where q_e (mg U/g sorbent) is the sorption capacity of U(VI), c_0 and c_e (mol L^{-1}) are the concentration of the U(VI) in the solution before and after sorption, respectively. V_s is the volume of the aqueous solution and m_s (g) is the dry weight of the sorbent.

Results and discussion

Characterization of the adsorbents

Low-angle X-ray powder diffraction pattern of SBA-15 and grafted SBA-15 were shown in Fig. 2. In the XRD pattern of SBA-15, there was an intense diffraction peak at about 0.8 degree and two plane and weak signals at about 1.5° and 1.75° respectively. The presence of (100) diffraction peaks as well as the weak (110) and (200) reflections indicate that all samples preserve the mesoscopic order after functionalization process [30].

Figure 3 shows FTIR spectra of SBA-15 before and after the modification. The typical peaks at 1080 and 804 and 461 cm^{-1} appear in the IR spectra of SBA-15, which are assigned to the Si–O–Si asymmetric stretching vibration, the Si–O–Si symmetric stretching vibration and Si–O–Si bending mode vibration respectively. The bands at 3435 and 1630 cm^{-1} are attributed to the hydrated silane group and bending vibrations of surface hydroxide [22, 31]. After the modification with amino groups, the FT-IR spectrum of modified SBA-15 displays a new peak at 2950–2850 cm^{-1}, which belongs to the stretching vibrations of C–H bond in alkyl chains [32]. They also presented characteristic bands for C–H of benzene ring stretching vibrations for pendant alkyl chains around 3000–2800 cm^{-1}. The new appeared several peaks at 1650–1430 cm^{-1} are related to C=C of benzene ring and C=N which indicated successful grafting of dihydroxy bezladely derivatives.

FT-IR spectra of adsorbents after adsorbed uranium are shown in Fig. 4. Compared with the materials before sorption, for SBA-15-OHBA, we can observe the UO_2^{2+} symmetric stretching vibrations at 944 cm^{-1} and the other two are at 950 and 949 cm^{-1} respectively. The peak of stretching vibrations of O=Si=O group at 1384 cm^{-1} have become more sharp. However, the rest adsorption bands remain constant.

The N_2 adsorption–desorption isotherm and BJH plot were exhibited as Fig. 5. In Fig. 5a, we could find that the isotherms of four kinds of materials have H1 hysteresis loop characteristic which belong to typical type IV. All isotherm exhibit a sharp capillary condensation step with the increasing p/p^0. According to the IUPAC classification, the characteristic of mesoporous materials [33, 34] indicate that all functionalized SBA-15 materials have reserved SBA-15 structure successfully. However, the BET, pore volume and pore size of modified SBA-15 have decreased gradually compared with pure SBA-15 (Table 1) [35, 36] because of the grafting reaction. The results indicate the

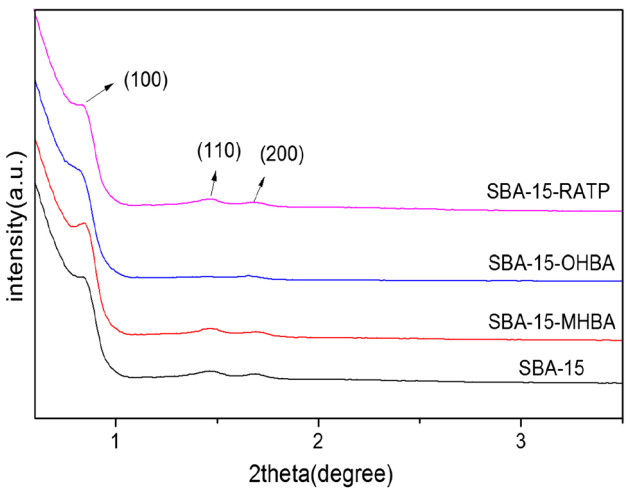

Fig. 2 XRD pattern of adsorbents

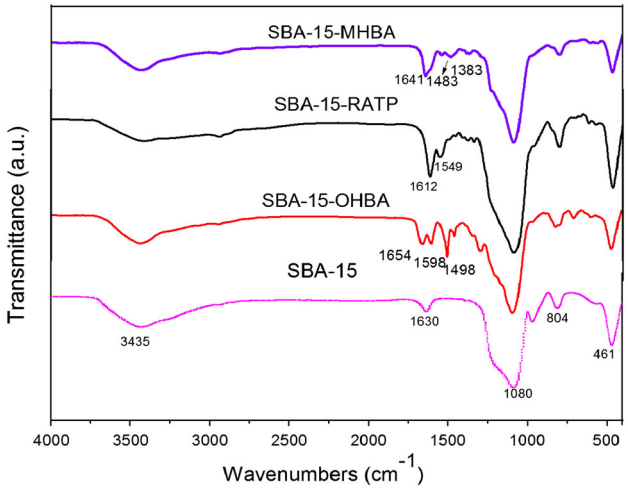

Fig. 3 FT-IR spectra of adsorbents

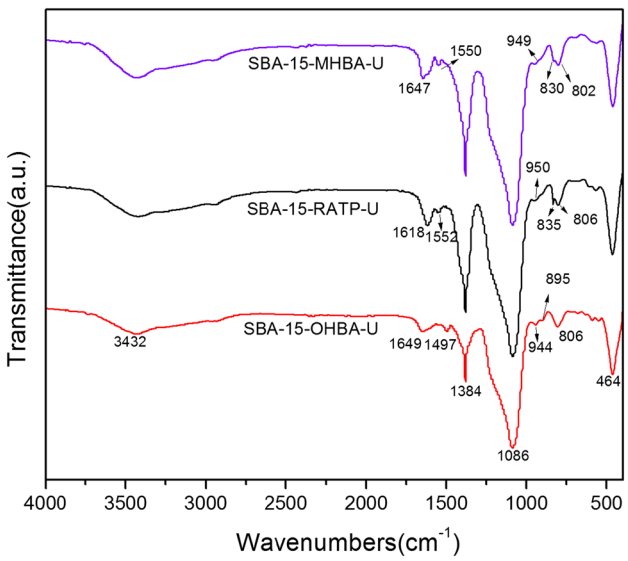

Fig. 4 FT-IR spectra of adsorbents after adsorbed uranium

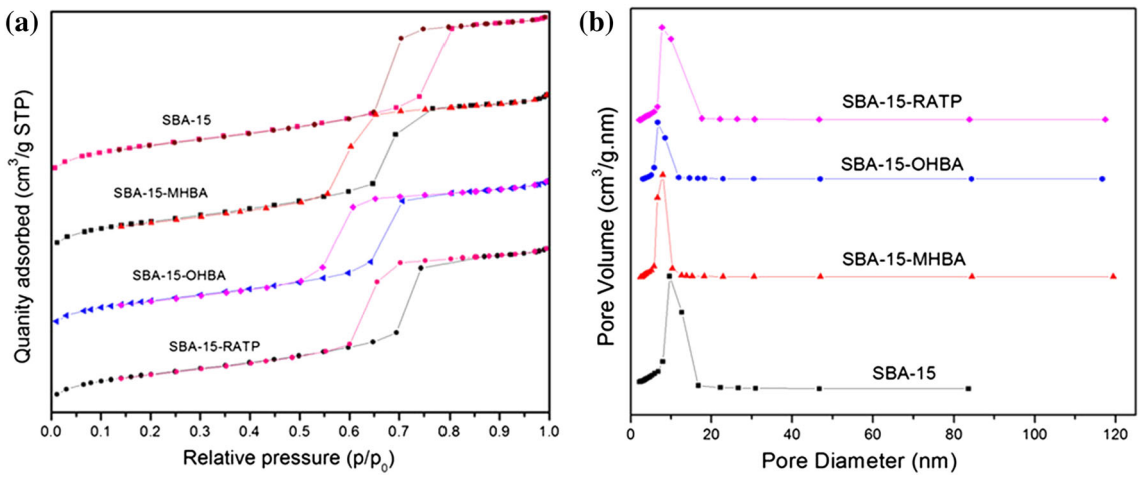

Fig. 5 **a** N_2 adsorption–desorption isotherms of pure and modified SBA-15 samples **b** BJH pore size distribution curves (acquired from the adsorption branch)

Table 1 Physical and chemical properties of adsorbents

	SBA-15	SBA-15-OHBA	SBA-15-MHBA	SBA-15-RATP
BET ($m^2\ g^{-1}$)	789.9	197.0	286.1	296.4
Pore volume ($cm^3\ g^{-1}$)	1.153	0.353	0.520	0.571
Pore size (nm)	7.590	6.840	6.915	7.469
C (wt%)	\	23.585	21.495	19.640
N (wt%)	\	2.155	2.810	2.325
H (wt%)	\	2.470	2.548	2.421
Functional groups content (mmol g^{-1})	\	1.539	2.007	1.661

successful grafting of organic groups onto the surfaces of SBA-15. The BJH plot of the derivatives of the pore volume per unit weight with respect to the pore diameter (*dV*/*dD*) versus the pore diameter is shown in Fig. 5b. A very narrow pore size distribution with an average pore diameter of 16 Å is observed.

Transmission electron microscopy (TEM) images are shown in Fig. 6. The TEM images suggested that the pure SBA-15 and functionalized SBA-15 particles have a well-ordered hexagonal array of mesoporous structure when the electron beam is paralled to the main axis of the cylindrical pores. When the electron beam is perpendicular to the main axis, the parallel nanotubular pores can be seen. It has been reported which the hexagonal array of SBA-15 materials is highly ordered and stable and these images also support this point. The TEM images confirmed that one-dimensional channels was made up of the hexagonal crystal structure [37–39]. What's more, it was demonstrated that the porous structure was not disrupted after the post-grafting reaction.

The contents of C, H and N for the mesoporous silica and the amount of functional groups grafted on the SBA-15 surface have been evaluated by element analysis. As can be observed from Table 1, the concentrations of functional groups for modified SBA-15 based on N elemental analysis for SBA-15-OHBA, SBA-15-MHBA and SBA-15-RATP were 1.539, 2.007 and 1.661 mmol g^{-1} respectively.

Figure 7 shows the ^{13}C CP-MAS NMR spectra of SBA-15-MHBA, SBA-15-OHBA and SBA-15-RATP. All the denoted peaks in the spectra can be assigned to appropriate C atoms. From the result, it can confirm that the mesoporous silica SBA-15 was functionalized by dihydroxy bezladely derivatives successfully [40, 41].

Sorption behavior studies of uranium

The effect of pH value on sorption of uranium

We have studied the parameters which affect the U(VI) adsorption properties of pure SBA-15 and grafted SBA-15 mesoporous silica. Figure 9 shows the effect of pH on sorption. From Fig. 9, the sorption ability of uranium by SBA-15 and composite materials are significantly dependent on the pH value. Because it affects the speciation of metal ions (Fig. 8), the surface charge and binding sites of the adsorbent [42].

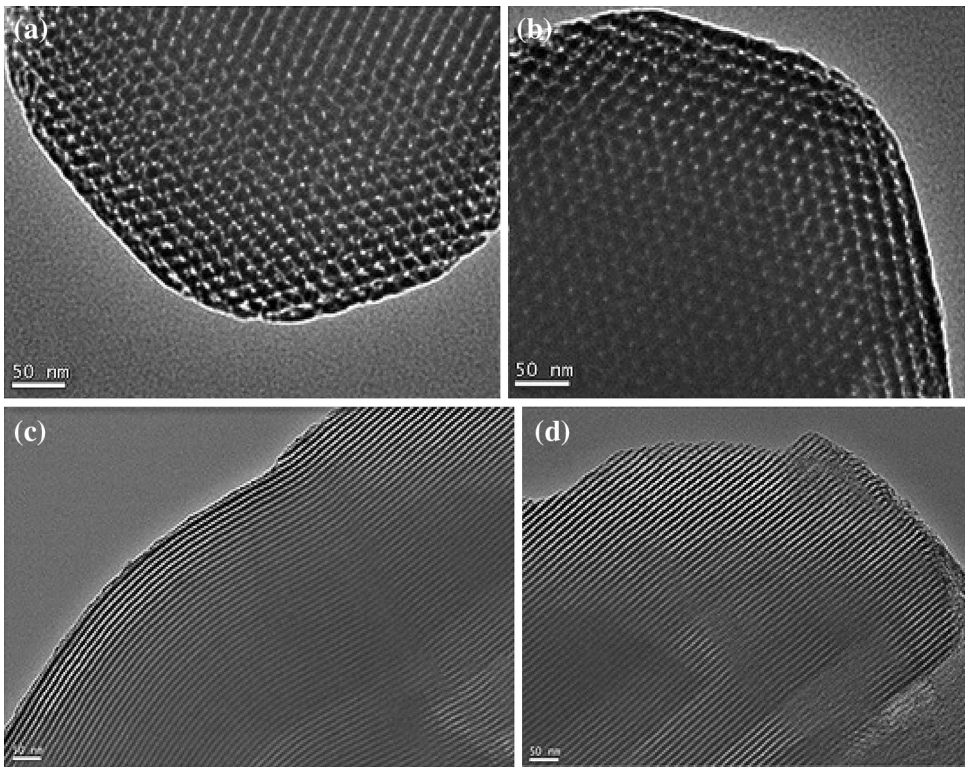

Fig. 6 TEM images of **a** SBA-15, **b** SBA-15-OHBA, **c** SBA-15-MHBA and **d** SBA-15-RATP

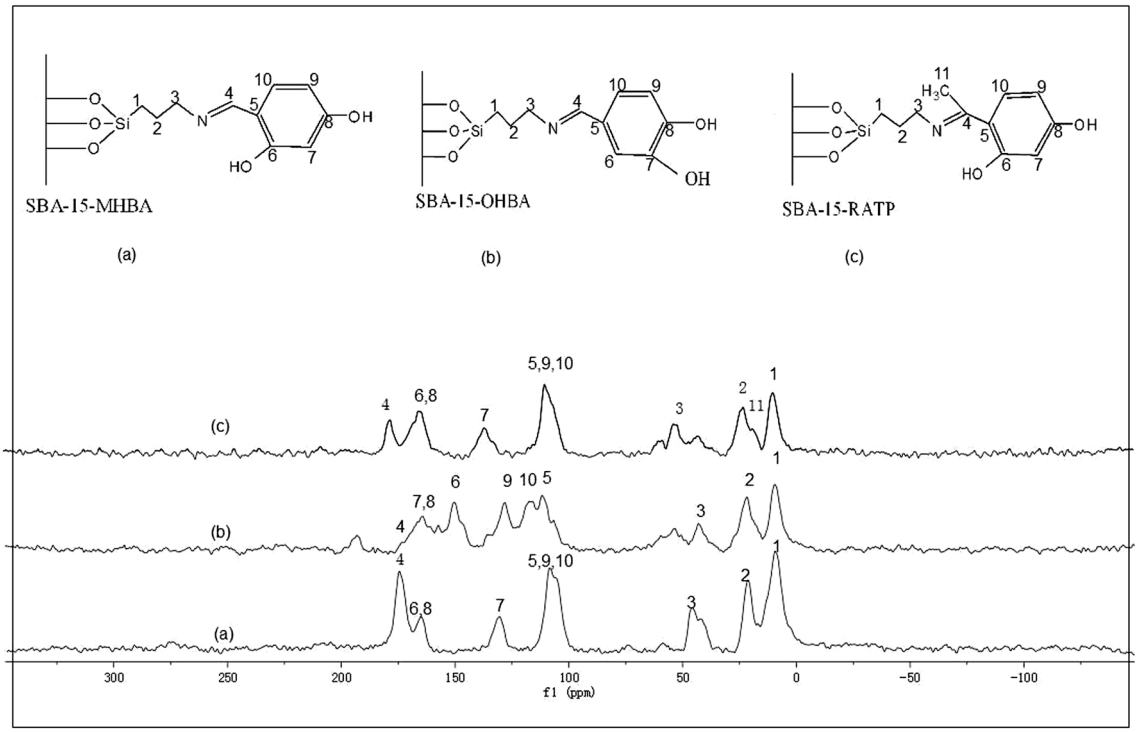

Fig. 7 Solid state ^{13}C CP-MAS NMR spectra of SBA-15-OHBA, SBA-15-MHBA and SBA-15-RATP

In our experiment, we choose the pH ranging from 1.5 to 7.0 [43]. The adsorption ability increases slightly with increasing pH ranging from 1.5 to 3 and then increases sharply to a maximum value with the rise of pH from 3.0 to 5.0. At last, sorption remain constant with further increase in pH. The effect of pH on uranium adsorption could be

explained by the surface characteristics of the adsorbents as well as the degree of ionization and speciation of the solute. When the pH was low, the U(VI) was present in the solution mainly in the form of free UO_2^{2+} ions and the binding sites of materials may become positively charged because of the protonation reaction resulting in the increase of electrostatic repulsion between U(VI) ions and materials. This effect decreases the adsorption capacity of U(VI) ions on the materials. With pH increasing, the surface of mesoporous silica are progressively deprotonated, exhibiting the anionic character. The attractive forces between the anionic surface sites and cationic uranyl ions easily result in the formation of metal–ligand magnetic composite complexes. However, when pH value is more than 5.0, schopite is formed along with other hydroxo species. On the basis of the above results, the optimum pH value is found to be 4.00 ± 0.02.

The ascending curves of the modified SBA-15 in Fig. 9 were wider, and the sorption percentage was higher than SBA-15. The sorption percentage increased with the increasing pH, which might be attributed to the presence of hydroxyl in 3, 4-dihydroxy benzaldehyde (OHBA), 2,4-dihydroxy benzaldehyde (MHBA) and 2,4-dihydroxyacetophenone (RATP) is suitable for coordination with U(VI).

Effect of the solid-to-liquid ratio

The effect of the solid-to-liquid ratio on the adsorption of U(VI) was investigated. Different amounts of solid-to-liquid ratio (from 0.125 to 3.5 g L^{-1}) were added to U(VI) solution with all other parameters keeping constant. It can be seen from Fig. 10 that the adsorption capacity increases rapidly with solid-to-liquid ratio value increasing at a lower value, while it increases slightly at a higher solid-to-liquid ratio for all materials. At last, the sorption rate keep constant with the solid-to-liquid ratio value increasing. The increase in adsorption capacity with increasing in the amount of adsorbent might be attributed to an increase in the surface area and the availability of adsorption sites of all materials for U(VI) [44, 45]. In addition, functionalized SBA-15 have a higher sorption ability than pure SBA-15 owing to more coordination sites in organic groups they have. SBA-15-OHBA, SBA-15-MHBA and SBA-15-RATP exhibit the similar adsorption efficiency, which could be due to the similar structural characteristics of functional groups on their surface.

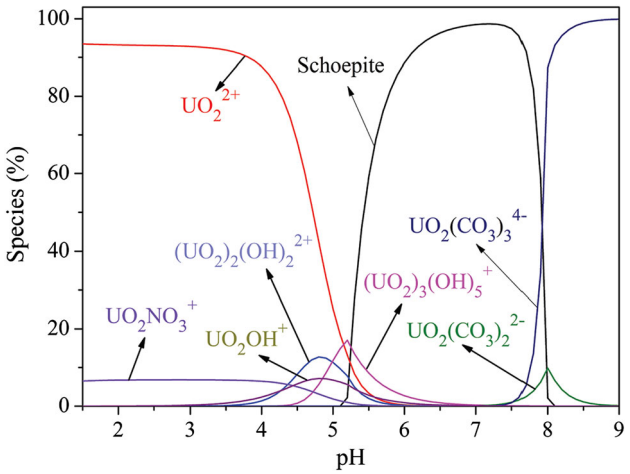

Fig. 8 The relative species distribution of UO_2^{2+} in the presence of CO_2 (by calculation). $C_{0U(VI)} = 2.00 \times 10^{-4}$ mol L^{-1}

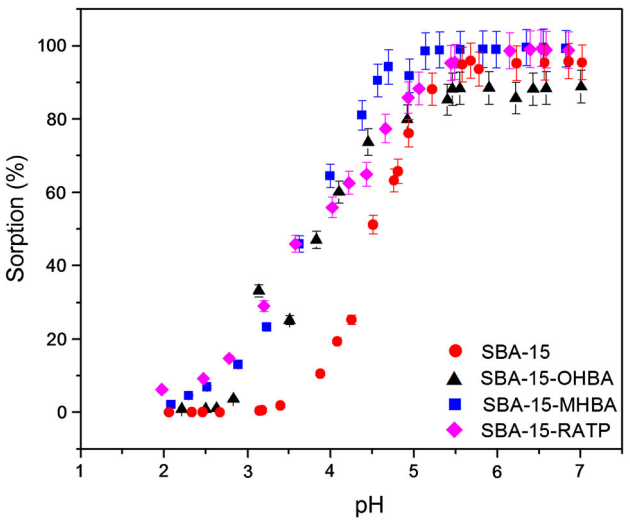

Fig. 9 The effect of pH values on sorption of uranium. $C_{0U(VI)} = 2.00 \times 10^{-4}$ mol L^{-1}, $m/V_{(SBA-15)} = 0.5$ g L^{-1}, $m/V_{(SBA-15-OHBA)} = 0.5$ g L^{-1}, $m/V_{(SBA-15-MHBA)} = 0.5$ g L^{-1}, $m/V_{(SBA-15-RATP)} = 0.5$ g L^{-1}, $C_{NaNO_3} = 0.1$ mol L^{-1}, $T = 298 \pm 1$ K, $t = 48$ h

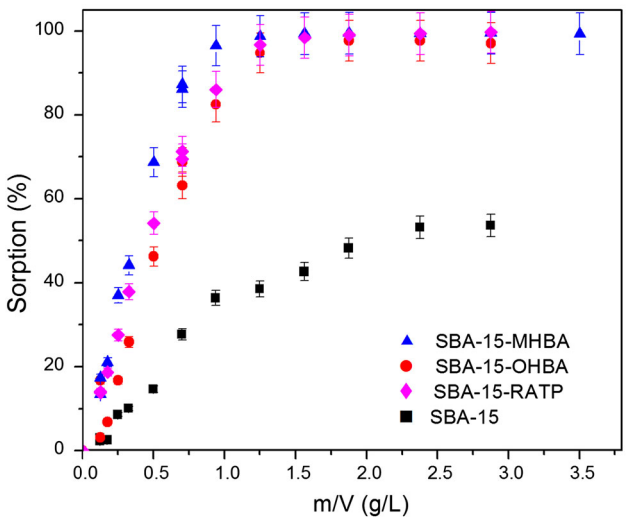

Fig. 10 The effect of the solid-to-liquid ratio on sorption of uranium. $C_{0U(VI)} = 2.00 \times 10^{-4}$ mol L^{-1}, $C_{NaNO_3} = 0.1$ mol L^{-1}, $T = 298 \pm 1$ K, pH = 4.00 ± 0.02, $t = 48$ h

Effect of ionic strength

Figure 11 shows the effect of ionic strength on the U(VI) sorption ability of four kinds of materials. Ionic strength is also an important parameter on the adsorption of U(VI). In Fig. 10, the percentage sorption of uranium decreases with the $NaNO_3$ concentration increasing from 0.01 to 0.10 mol L^{-1}. Then remains constant when the concentration of $NaNO_3$ was higher than 0.1 mol L^{-1}. From these phenomena, we could see that the adsorption rate remains nearly constant indicating negligible effect of ionic strength on the adsorption process. This suggests that the sorption process follows inner sphere complex formation between U(VI) and surface sites on mesoporous silica. The reason why small decrease in the percentage sorption with increasing ionic strength (I) up to $I = 0.1$ M might be the ionic strength dependence of the binding constant of U(VI) with silica [46, 47].

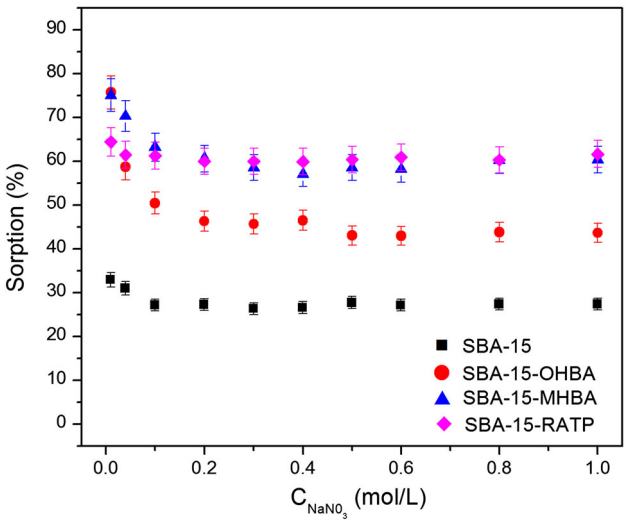

Fig. 11 The effect of ionic strength on the sorption of U(VI). $C_{0U(VI)} = 2.00 \times 10^{-4}$ mol L^{-1}, $m/V_{(SBA\text{-}15)} = 0.5$ g L^{-1}, $m/V_{(SBA\text{-}15\text{-}OHBA)} = 0.5$ g L^{-1}, $m/V_{(SBA\text{-}15\text{-}MHBA)} = 0.5$ g L^{-1}, $m/V_{(SBA\text{-}15\text{-}RATP)} = 0.5$ g L^{-1}, $T = 298 \pm 1$ K, pH $= 4.00 \pm 0.02$, $t = 48$ h

Time-dependent sorption

For the economic efficiency, the sorption ability is an important factor in evaluating the overall performance of sorbents. As shown in Fig. 12a, the sorption rate of U(VI) on pure and grafted SBA-15 increases rapidly in the contact time of 180 min and then increases slightly until the sorption equilibrium is attained. Application of proper kinetic models to fit the experimental kinetic data can offer useful information to identify the sorption mechanism type. Therefore, we have used pseudo first-order and pseudo second-order models (Fig. 12b) for their validity with the experimental sorption data for U(VI). The linear forms of pseudo first-order and pseudo second-order kinetic models are given as follows [48]:

$$\ln(q_e - q_t) = \ln(q_e) - k_1 t \quad ((3))$$

$$\frac{t}{q_t} = \frac{1}{k_2 \cdot q_e^2} + \frac{t}{q_e} \quad ((4))$$

where q_t (mol g^{-1}) and q_e (mol g^{-1}) are the sorption amounts of U(VI) ions at contact time of t (min) and at equilibrium time, respectively; k_1 (min^{-1}) and k_2 (g mol^{-1} min^{-1}) represent the pseudo first-order and the pseudo second-order sorption rate constants. The factors of the kinetic models and the correlation coefficient (R^2) are listed in Table 2. It could be found that the experimental data was

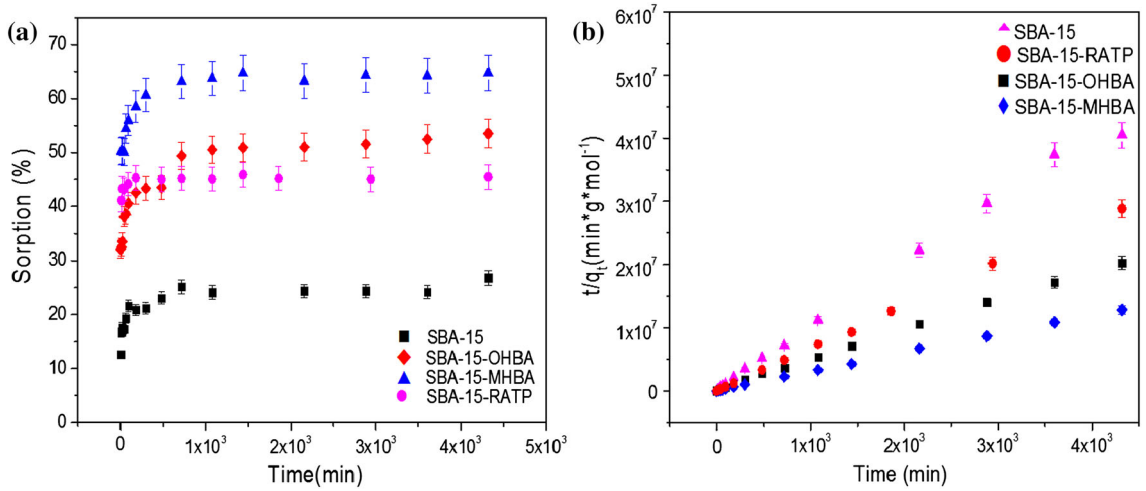

Fig. 12 **a** The effect of contact time on U(VI) adsorption ability to adsorbents. $C_{NaNO_3} = 0.1$ mol L^{-1}, $m/V_{(SBA\text{-}15,\ SBA\text{-}15\text{-}OHBA,\ SBA\text{-}15\text{-}MHBA,\ SBA\text{-}15\text{-}RATP)} = 0.5$ g L^{-1}, $T = 298 \pm 1$ K, pH $= 4.00 \pm 0.02$, $t = 48$ h. **b** Pseudo second-order sorption kinetics of U(VI) on adsorbents

fitted very well to the pseudo second-order model from the R^2 values. The results of pseudo second-order kinetics further imply that the sorption mechanism of adsorbate (U(VI)) and adsorbent are chemisorption.

Adsorption isotherms

The influence of temperature on sorption of U(VI) was investigated at different temperatures 298, 318 and 338 K

Table 2 Kinetic sorption parameters obtained using pseudo first-order and pseudo second-order models for U(VI) sorption on adsorbents

	Pseudo first-order					
	q_e (mol g^{-1})	Unc.	k (min^{-1})	Unc.	R^2	Unc.
SBA-15	1.07E−4	5.35E−06	4.00E−4	2.00E−05	0.4875	0.0244
SBA-15-OHBA	2.13E−4	1.07E−05	7.00E−4	3.50E−05	0.5726	0.0286
SBA-15-MHBA	3.36E−4	1.68E−05	9.00E−4	4.50E−05	0.8075	0.0404
SBA-15-RATP	1.54E−4	7.70E−06	3.00E−4	1.50E−05	0.4193	0.0210
	Pseudo second-order					
	q_e (mol g^{-1})	Unc.	k (g mol^{-1} min^{-1})	Unc.	R^2	Unc.
SBA-15	1.02E−4	5.10E−06	2.778E+2	13.890	0.9965	0.0498
SBA-15-OHBA	2.11E−4	1.06E−05	1.181E+2	5.905	0.9993	0.0500
SBA-15-MHBA	3.35E−4	1.68E−05	1.034E+2	5.170	0.9997	0.0500
SBA-15-RATP	1.49E−4	7.45E−06	1.072E+3	53.600	0.9996	0.0500

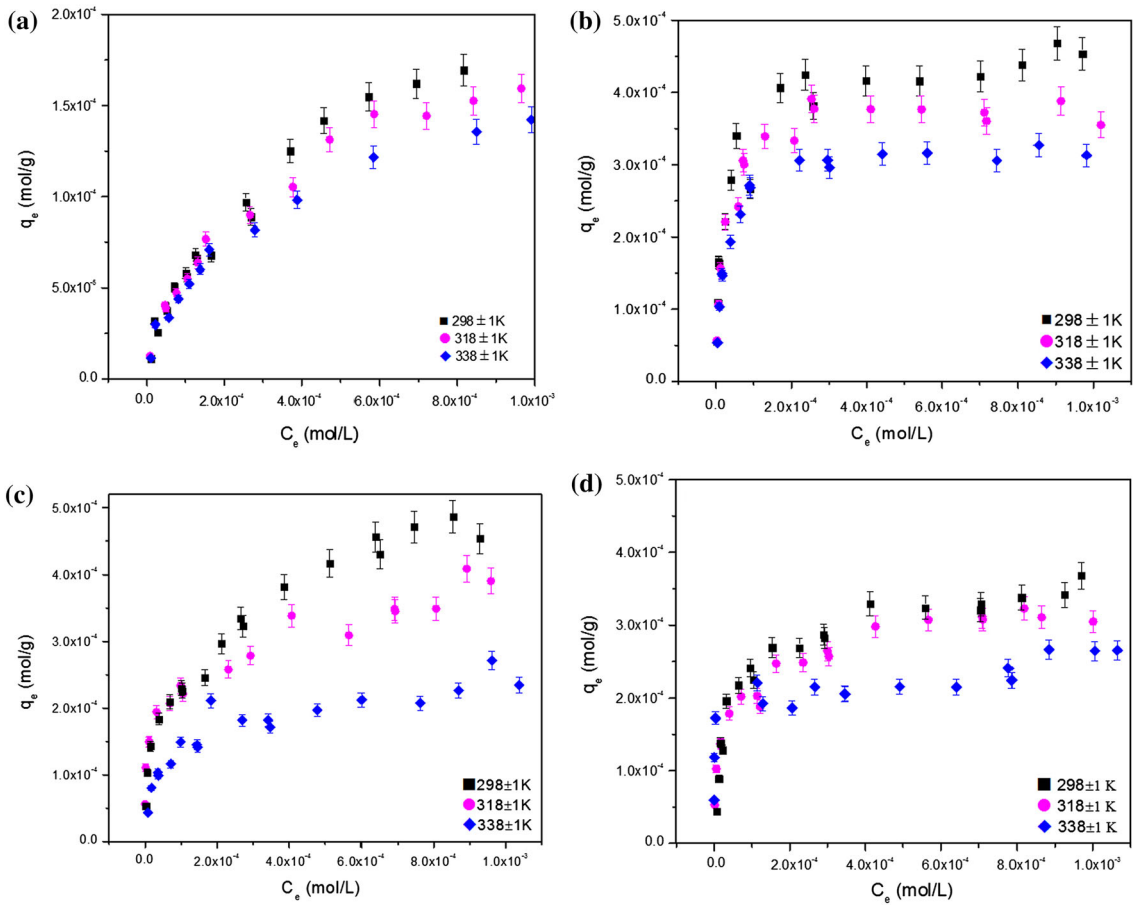

Fig. 13 Sorption isotherms of U(VI) onto **a** SBA-15, **b** SBA-15-MHBA, **c** SBA-15-OHBA, **d** SBA-15-RATP. $C_{NaNO_3} = 0.1$ mol L^{-1}, $m/V_{(SBA-15)} = 0.5$ g L^{-1}, $m/V_{(SBA-15-OHBA)} = 0.5$ g L^{-1}, $m/V_{(SBA-15-MHBA)} = 0.5$ g L^{-1}, $T = 298 \pm 1$ K, pH $= 4.00 \pm 0.02$, $t = 48$ h

(Fig. 13). Figure 13 shows that the sorption ability for all materials increases with the increasing concentration of U(VI). In addition, the U(VI) sorption ability of SBA-15 decreased with the increasing temperature, demonstrating that the sorption process is an exothermic process. For functionalized SBA-15 materials, the sorption ability decreased with the temperature increasing, indicating that the sorption was an exothermic process for these materials too. Adsorption isotherm plays a crucial role in the physicochemical behavior of metal ions. Adsorption isotherm can prove how the adsorbate molecules distribute between the liquid and the solid phases when the sorption process reaches an equilibrium state. Therefore, using Freundlich (Fig. 14a) and Langmuir (Fig. 14a) equations which are most common mathematical models to describe the correlation of equilibrium data are important to the practical design and operation of adsorption systems.

The expression of the Langmuir model is given by Eq. (5) [49]:

$$\frac{C_e}{q_e} = \frac{C_e}{q_{max}} + \frac{1}{K_L} \tag{5}$$

where K_L is a adsorption equilibrium constant, C_e is the equilibrium concentration (mol L^{-1}), q_e is the amount adsorbed at equilibrium (mol g^{-1}), q_m is the the maximum sorption capacity (mol g^{-1}).

The Freundlich model can be represented in the linearized form as Eq. (6):

$$\lg q_e = \lg K_F + n \lg C_e \tag{6}$$

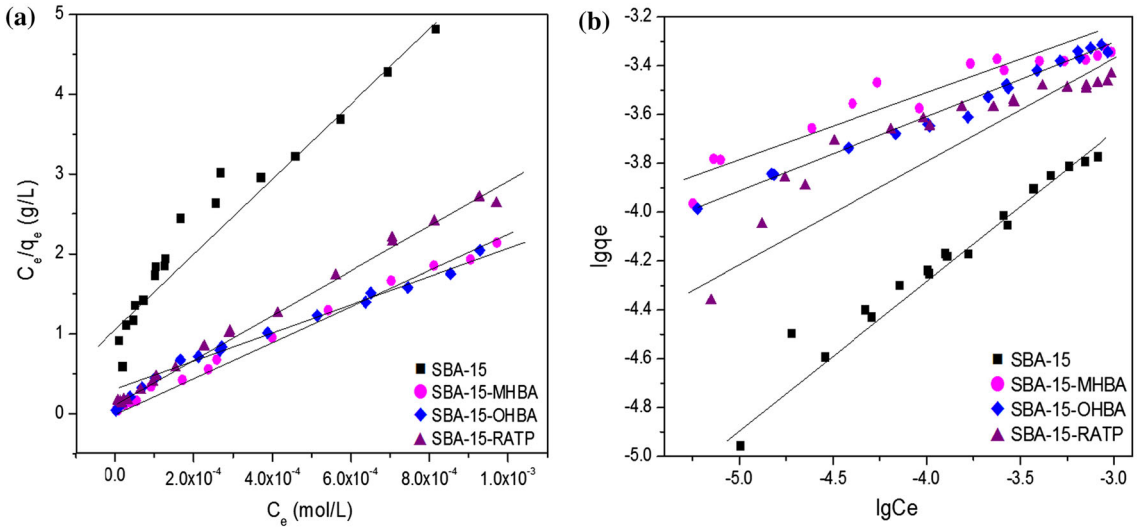

Fig. 14 The isotherms of **a** Langmuir and **b** Freundlich models for U(VI) sorption. $C_{NaNO_3} = 0.1$ mol L^{-1}, $m/V = 0.5$ g L^{-1}, $T = 298 \pm 1$ K, pH = 4.00 ± 0.02, $t = 48$ h

Table 3 Sorption parameters of U(VI) sorption to the adsorbents ($T = 298 \pm 1$ K)

Samples	Langmuir constants					
	q_{max} (mol g^{-1})	Unc.	K_L (L g^{-1})	Unc.	R^2	Unc.
SBA-15	2.1294E−04	1.0647E−05	0.8610	0.0431	0.9678	0.0484
SBA-15-MHBA	4.5939E−04	2.2970E−05	15.9490	0.7975	0.9962	0.0498
SBA-15-OHBA	5.0246E−04	2.5123E−05	5.5741	0.2787	0.9767	0.0488
SBA-15-RATP	3.6142E−04	1.8071E−05	6.9541	0.3477	0.9948	0.0497
Samples	Freundlich constants					
	K_F (mol^{1-n} L^n g^{-1})	Unc.	n	Unc.	R^2	Unc.
SBA-15	1.08E−02	5.40E−04	0.5652	0.0283	0.9749	0.0487
SBA-15-MHBA	3.75E−03	1.88E−04	0.2800	0.0140	0.8608	0.0430
SBA-15-OHBA	5.03E−03	2.52E−04	0.3323	0.0166	0.9769	0.0488
SBA-15-RATP	3.67E−03	1.84E−04	0.3175	0.0159	0.8390	0.0420

where K_F ($mol^{1-n}\ L^n\ g^{-1}$) represents the sorption capacity when the adsorbate equilibrium concentration equals 1, and n is the degree of sorption dependence at equilibrium concentration [50].

The adsorption constants of the Langmuir and Freundlich equation and their correlation coefficients (R^2) at 298, 318, and 338 K are calculated and presented in Table 3. From the results, we can find that there is a good improvement in maximum sorption capacity compared with pure SBA-15 for functionalized SBA-15.

Selectivity studies

In order to evaluate the selectivity of pure and functionalized SBA-15 materials, selective sorption of U(VI) studies were carried out in aqueous solution containing other competitive metal ions. In the research of selectivity, the tests were performed in aqueous solution containing UO_2^{2+}, Ca^{2+}, Co^{2+}, K^+, Mg^{2+}, Sr^{2+}, Cd^{2+} at pH 4.00 ± 0.02. The amount of residual coexisting metal ions in supernatants after adsorption were determined by ICP-AES. The results in Fig. 15 show that SBA-15-MHBA, SBA-15-OHBA and SBA-15-RATP exhibit a better sorption efficiency for U(VI) than pure SBA-15. From the results, it indicates that the presence of Ca^{2+}, K^+, Co^{2+}, Cd^{2+}, Sr^{2+} and Mg^{2+} have no significant effect on adsorption of U(VI) on modified SBA-15. The results suggest that all mesoporous materials have higher sorption ability for U(VI) and lower sorption ability for competing metal ions. It is worth mentioning that, the selective sorption ability of SBA-15-MHBA and SBA-15-RATP may have promising application in U(VI) separation field.

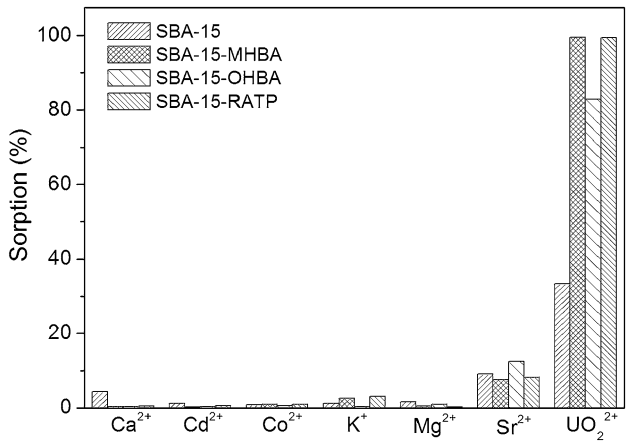

Fig. 15 Competitive sorption of coexisting ions. $C_{0U(VI)} = 1.25 \times 10^{-4}$ mol L − 1, $C_{0K(I)} = 2.58 \times 10^{-3}$ mol L^{-1}, $C_{0Ca(II)} = 3.58 \times 10^{-3}$ mol L^{-1}, $C_{0Mg(II)} = 3.42 \times 10^{-3}$ mol L^{-1}, $C_{0Cd(II)} = 2.50 \times 10^{-3}$ mol L^{-1}, $C_{0Co(II)} = 3.48 \times 10^{-3}$ mol L^{-1}, $C_{0Sr(II)} = 3.65 \times 10^{-3}$ mol L^{-1}, $C_{NaNO_3} = 0.1$ mol L^{-1}, $m/V = 0.5$ g L^{-1}, pH = 4.00 ± 0.02, $T = 298 \pm 1$ K, $t = 48$ h

Desorption and reusability experiments

To get a better study of the modified mesoporous silicas, the tests on desorption and reusability of SBA-15-OHBA, SBA-15-MHBA and SBA-15-RATP are essential. Desorption experiments were operated after the adsorption equilibrium, both of them were adopted under the same adsorption experimental conditions: $C_{0U(VI)} = 4.00 \times 10^{-4}$ mol L^{-1}, $m/V = 2.0$ g L^{-1}, $C_{NaNO_3} = 0.1$ mol L^{-1}, $T = 298 \pm 1$ K.

The U(VI) desorption rate from modified SBA-15 were studied as a function of pH value (pH values of the solution were adjusted using NaOH and HNO_3 solutions). From

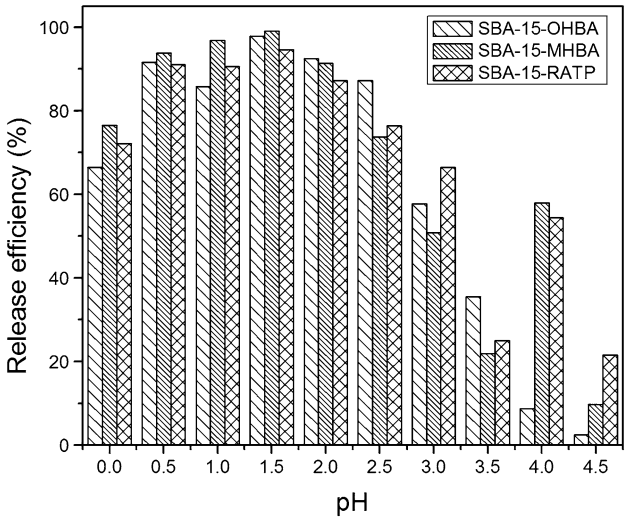

Fig. 16 Release efficiencies of U(VI) versus pH on SBA-15-MHBA, SBA-15-OHBA, SBA-15-RATP in solutions

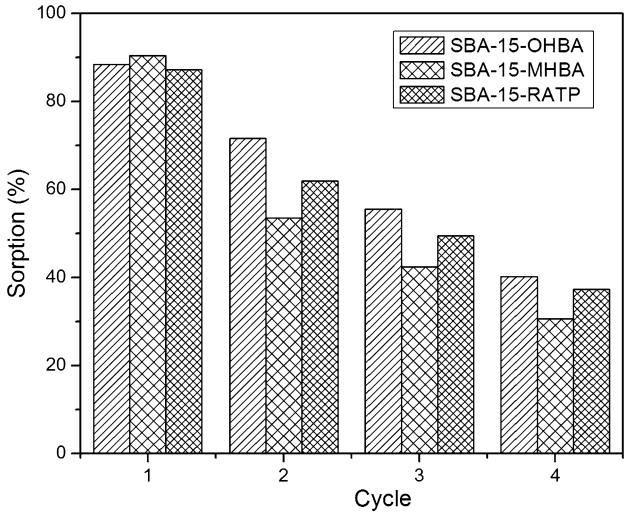

Fig. 17 Reusability tests of SBA-15-MHBA, SBA-15-OHBA, SBA-15-RATP

Fig. 16, it is clear that when the pH value was 1.5, release percent of U(VI) was the highest. The reusability test of three materials were conducted in the same operating conditions of sorption study at first. Then doing desorption study in HNO_3 solutions (pH = 1.5). As seen from Fig. 17, the capacities of three modified materials reduced with the increase of repeating times.

Conclusions

In this study, three different dihydroxy bezladely derivatives functionalized mesoporous silica SBA-15 materials have been successfully synthesized and their sorption for U(VI) from aqueous solutions were studied by batch sorption experiment. From the results, it could be seen that higher adsorption affinity for aqueous U(VI) was achieved after the modification for pure SBA-15, the sorption ability for U(VI) relies heavily on pH values before and after the functionalization. The sorption mechanism of U(VI) might be inner-sphere complexation from the research of effect of ionic strength. The adsorption process for all materials were follow pseudo-second-order type sorption kinetics. The sorption isotherm for pure SBA-15 has been successfully modeled by the Freundlich isotherm which indicated that different sites with several sorption energies were involved. However, for three different modified SBA-15 the Langmuir isotherm was better and it revealed a monolayer chemical sorption of U(VI) on modified SBA-15. SBA-15-MHBA and SBA-15-RATP showed a good sorption ability and a desirable selectivity for U(VI) over a range of competing metal ions.

Acknowledgments This work was supported by National Natural Science Foundation of China (21101082, J1210001) and Fundamental Research Funds for the Central University (Lzujbky-2013-55).

References

1. DeCanio SJ, Fremstad A (2011) Economic feasibility of the path to zero net carbon emissions Original. Energy Policy 39: 1144–1153
2. Zhang YY, Zhao HG, Fan QH, Zheng XJ, Li P, Liu SP, Wu WS (2011) Sorption of U(VI) onto a decarbonated calcareous soil. J Radioanal Nucl Chem 288:395–404
3. Akyil S, Aslani MAA, Eral M (2003) Sorption characteristics of uranium onto composite ion exchangers. J Radioanal Nucl Chem 256:45–51
4. Wazne M, Korfiatis GP, Meng XG (2003) Carbonate effects on hexavalent uranium adsorption by iron oxyhydroxide. Environ Sci Technol 37:3619–3624
5. Ilton ES, Wang ZM, Boily JF, Qafoku O, Rosso KM, Smith SC (2012) The effect of pH and time on the extractability and speciation of uranium(VI) sorbed to SiO_2. Environ Sci Technol 46:6604–6611
6. Bazykav DA, Prysyazhnyuk AY, Romanenko AY, Fedorenko ZP, Gudzenko NA, Fuzik MM, Khukhrianska OM, Trotsyuk NK, Gulak LO, Goroch YL, Sumkina YV (2012) Cancer incidence and nuclear facilities in ukraine: a community-based study. Exp Oncol 34:116–120
7. Brugge D, Lemos JL, Oldmixon B (2010) Exposure pathways and health effects associated with chemical and radiological toxicity of natural uranium: a review. Rev Environ Health 20:177–194
8. Kumari N, Prabhu DR, Pathak PN, Kanekar AS, Manchanda VK (2011) Extraction studies of uranium into a third-phase of thorium nitrate employing tributyl phosphate and *N*, *N*-dihexyl octanamide as extractants in different diluents. J Radioanal Nucl Chem 289:835–843
9. Hu BW, Cheng W, Zhang H, Sheng GD (2010) Sorption of radionickel to goethite: effect of water quality parameters and temperature. J Radioanal Nucl Chem 285:389–398
10. Hanif HA, Nadeem R, Bhatti HN, Ahmad NR, Ansari TM (2007) Ni(II) biosorption by Cassia fistula (Golden Shower) biomass. J Hazard Mater 139:345–355
11. Satapathy D, Natarajan GS (2006) Potassium bromate modification of the granular activated carbon and its effect on nickel adsorption. Adsorption 12:147–154
12. Wang XJ, Xia SQ, Chen L, Zhao JF, Chovelon J, Nicole J (2006) Biosorption of cadmium(II) and lead(II) ions from aqueous solutions onto dried activated sludge. J Environ Sci 18:840–844
13. Manos MJ, Kanatzidis MG (2012) Layered metal sulfides capture uranium from seawater. J Am Chem Soc 134:16441–16446
14. Comarmond MJ, Payne TE, Harrison JJ, Thiruvoth S, Wong HK, Aughterson RD, Lumpkin GR, Muller K, Foerstendorf H (2011) Uranium sorption on various forms of titanium dioxide—influence of surface area, surface charge, and impurities. Environ Sci Technol 45:5536–5542
15. Ying YL, Mehnert CP, Wong MS (1999) Synthesis and applications of supramolecular-templated mesoporous materials. Angew Chem 38:56–77
16. Øye G, Sjöblom J, Stöcker M (2001) Synthesis, characterization and potential applications of new materials in the mesoporous range. Adv Colloid Interface Sci 89:439–466
17. On DT, Desplantier-Giscard D, Danumah C, Kaliaguine S (2001) Perspectives in catalytic applications of mesostructured materials. Appl Catal A 222:299–357
18. Kresge CT, Leonowicz ME, Roth WJ (1992) Ordered mesoporous molecular sieves synthesized by a liquid-crystal template mechanism. Nature 359:710–712
19. Beck JS, Vartuli JC, Roth WJ, Leonowicz ME, Kresge CT, Schmitt KD, Chu CTW, Olson DH, Sheppard EW, Cullen SBM, Higgins JB, Schlenker JL (1992) A new family of mesoporous molecular sieves prepared with liquid crystal templates. J Am Chem Soc 114:10834–10843
20. Li M, Pham PJ, Pittman CU, Li T (2009) SBA-15-supported ionic liquid compounds containing silver salts: novel mesoporous π-complexing sorbents for separating polyunsaturated fatty acid methyl esters. Microporous Mesoporous Mater 117:436–443
21. Wang YL, Song LJ, Zhu L, Guo BL, Chen SW, Wu WS (2014) Removal of uranium(VI) from aqueous solution using iminodiacetic acid derivative functionalized SBA-15 as adsorbents. Dalton Trans 43:3739
22. Quintanilla DP, Hierro ID, Fajardo M, Sierra I (2006) 2-Mercaptothiazoline modified mesoporous silica for mercury removal from aqueous media. J Hazard Mater 134:245–256
23. Mureseanu M, Reiss A, Cioatera N, Trandafir I, Hulea V (2010) Mesoporous silica functionalized with 1-furoyl thiourea urea for Hg(II) adsorption from aqueous media. J Hazard Mater 182:197–203

24. Wang YL, Zhu L, Guo BL, Chen SW, Wu WS (2014) Mesoporous silica SBA-15 functionalized with phosphonate derivatives for uranium uptake. New J Chem 38:3853
25. Yantasee W, Fryxell GE, Addleman RS, Wiacek RJ, Koonsiripaiboon V, Pattamakomsan K, Sukwarotwat V, Xu J, Raymond KN (2009) Selective removal of lanthanides from natural waters, acidic streams and dialysate. J Hazard Mater 168: 1233–1238
26. Anupama G, Ajai KS (2002) Silica gel functionalized with resacetophenone: synthesis of a new chelating matrix and its application as metal ion collector for their flame atomic absorption spectrometric determination. Anal Chim Acta 454:229–240
27. Mahmoud ME, Soliman EM (1997) Silica-immobilized formylsalicylic acid as a selective phase for the extraction of iron(III). Talanta 44:15–22
28. José A, Jesús MA, Amaya A, Montaña L, Victoria G (2009) Aqueous heavy metals removal by adsorption on amine-functionalized mesoporous silica. J Hazard Mater 163:213–221
29. Gao L, Yang Z, Shi K, Wang X, Guo Z, Wu W (2010) U(VI) sorption on kaolinite: effects of pH, U(VI) concentration and oxyanions. J Radioanal Nucl Chem 284:519–526
30. José A, Jesús MA, Amaya A, Montaña L, Victoria G (2009) Aqueous heavy metals removal by adsorption on amine-functionalized mesoporous silica. J Hazard Mater 163:213–221
31. Tao Q, Xu ZY, Wang JH, Liu FL, Wan HQ, Zheng SR (2010) Adsorption of humic acid to aminopropyl functionalized SBA-15. Microporous Mesoporous Mater 131:177–185
32. Kleitz F, Bérubé F, Guillet-Nicolas R, Yang CM, Thommes M (2010) Probing adsorption, pore condensation, and hysteresis behavior of pure fluids in three-dimensional cubic mesoporous KIT-6 silica. J Phys Chem C 114:9344–9355
33. Kim TW, Kleitz F, Paul B, Ryoo R (2005) MCM-48 like large mesoporous silicas with tailored pore structure: facile synthesis domain in a ternary triblock copolymer-butanol-water system. J Am Chem Soc 127:601–7610
34. Sevimli F, Yilmaz A (2012) Surface functionalization of SBA-15 particles for amoxicillin delivery. Microporous Mesoporous Mater 158:281–291
35. Njoku VO, Foo KY, Asif M, Hameed BH (2014) Preparation of activated carbons from rambutan (Nephelium lappaceum) peel by microwave-induced KOH activation for acid yellow 17 dye adsorption. Chem Eng J 250:198–204
36. Wang L, Yang RT (2011) Increasing selective CO2 adsorption on amine-grafted SBA-15 by increasing silanol density. J Phys Chem C 115:21264–21272
37. Hernández-Morales V, Nava R, Acosta-Silva YJ, Macías-Sánchez SA, Pérez-Bueno JJ, Pawelec B (2012) Adsorption of lead(II) on SBA-15 mesoporous molecular sieve functionalized with $-NH_2$ groups. Microporous Mesoporous Mater 160:133–142
38. Yang Y, Zhang Y, Hao SL, Kan QB (2011) Tethering of Cu(II), Co(II) and Fe(III) tetrahydro-salen and salen complexes onto amino-functionalized SBA-15: effects of salen ligand hydrogenation on catalytic performances for aerobic epoxidation of styrene. Chem Eng J 171:1356–1366
39. Gao ZF, Wang LN, Qi T, Chu JL, Zhang Y (2007) Synthesis, characterization, and cadmium(II) uptake of iminodiacetic acid-modified mesoporous SBA-15. Colloids Surf A 304:77–81
40. Przybylski P, Schilf W, Brzezinski B (2005) ^{13}C, ^{15}N NMR and CP-MAS as well as FT-IR and PM5 studies of Schiff base of gossypol with L-phenylalanine methyl ester in solution and solid. J Mol Struct 734:123–128
41. El-Nahhal IM, Zaggout FR, Nassar MA (2003) Synthesis, characterization and applications of immobilized iminodiacetic acid-modified silica. J Sol-Gel Sci Technol 28:255–265
42. Nie BW, Zhang ZB, Cao XH, Liu YH, Liang P (2012) Sorption study of uranium from aqueous solution on ordered mesoporous carbon CMK-3. J Radioanal Nucl Chem 295:663–670
43. Yang Y, Zhang Y, Hao S, Kan Q (2011) Tethering of Cu(II), Co(II) and Fe(III) tetrahydro-salen and salen complexes onto amino-functionalized SBA-15: effects of salen ligand hydrogenation on catalytic performances for aerobic epoxidation of styrene. Chem Eng J 171:1356–1366
44. Shao DD, Fan QH, Li JX, Niu ZW, Wu WS, Chen YX, Wang XK (2009) Removal of Eu(III) from aqueous solution using ZSM-5 zeolite. Microporous Mesoporous Mater 123:1–9
45. Chen CL, Wang XK (2007) Influence of pH, soil humic/fulvic acid, ionic strength and foreign ions on sorption of thorium(IV) onto γ-Al_2O_3. Appl Geochem 22:436–445
46. Kar AS, Kumar S, Tomar BS_*, Manchanda VK (2011) Sorption of curium by silica colloids: effect of humic acid. J Hazard Mater 186:1961–1965
47. Dzombak DA, Morel FMM (1990) Surface complexation modeling: hydrous ferric oxide. Wiley, New York
48. Tian G, Geng JX, Jin YD, Wang CL, Li SQ, Chen Z, Wang H, Zhao YS, Li SJ (2011) Sorption of uranium(VI) using oxime-grafted ordered mesoporous carbon CMK-5. J Hazard Mater 190:442–450
49. Chen CL, Li XL, Zhao DL, Tan XL, Wang XK (2007) Application of oxidized multi-wall carbon nanotubes for Th(IV) adsorption. Radiochim Acta 95:261–266
50. Semnani F, Asadi Z, Samadfam M, Sepehrian H (2012) Uranium(VI) sorption behavior onto amberlite CG-400 anion exchange resin: effects of pH, contact time, temperature and presence of phosphate. Ann Nucl Energy 48:21–24